Hindawi
Complexity
Volume 2020, Article ID 9015923, 13 pages
https://doi.org/10.1155/2020/9015923

Research Article

A Least Cumulative Ventilation Cost Method for Urban Ventilation Environment Analysis

Peng Xie, Dianfeng Liu, Yanfang Liu, and Yaolin Liu

School of Resource and Environmental Science, Wuhan University, 129 Luoyu Road, Wuhan 430079, Hubei Province, China

Correspondence should be addressed to Yanfang Liu; yfliu610@163.com and Yaolin Liu; yaolin610@163.com

Received 31 January 2020; Accepted 15 April 2020; Published 12 May 2020

Guest Editor: Jianhong (Cecilia) Xia

The correct urban building layout is an important influencing factor in urban ventilation, and the heat island effect has become an important factor affecting the quality of urban life. Optimization of the urban building layout can play a role in mitigating the heat island effect. The traditional ventilation corridor analysis method, based on a least-cost path analysis, can only generate a few main ventilation corridors. It is difficult to obtain global ventilation results covering the whole study area using this method of analysis. On the basis of urban morphology and a least-cost path analysis, this study proposes a "least cumulative ventilation cost" method for analyzing urban ventilation. Taking Wuhan downtown as a research area, the urban ventilation environment under different wind directions and seasons was analyzed. This method can effectively express the ventilation conditions throughout the whole study area and can simultaneously express the quality of the generated corridors effectively. The results show that Wuhan has three levels of ventilation corridor. Moreover, the ventilation conditions in Wuchang (Wuchang, Qingshan, and Hongshan) are better than those in Hankou (Qiaokou, Jianghan, and Jiang'an).

1. Introduction

The urban heat island (UHI) effect is a phenomenon in which heat accumulates in an urban area due to people's activities and the buildings. It is one of the most prominent characteristics of the urban climate. With rapid urbanization and a continuous increase in population density, the UHI effect has become an important adverse factor affecting the quality of urban life [1–5]. UHI effects caused by high-density urban buildings have been reported around the world; it has changed the urban thermal environment [6–10]. As a result of its effects on regional climates, urban hydrology, air quality, urban biological distribution and behavior, and many urban ecological processes, the UHI effect has raised a number of ecological and environmental issues [11–15]. Numerous studies have found that the effect is closely related to urban anthropogenic heat release, underlying surface properties and structure, vegetation coverage, population density, and weather conditions. Among many factors, urban ventilation conditions caused by the underlying surface properties and structure have a significant impact on the UHI effect [16–20]. In order for governments and city planners to make planning decisions intuitively, quantitative methods are needed to determine ventilation paths in urban planning [21–23].

The most common simulation methods of urban canopy ventilation corridors use wind tunnels, computational fluid dynamics (CFD), and morphological analysis based on GIS technology. Wind tunnels can be used for wind environment simulations at various scales [24–26]. Although wind tunnel simulations can objectively and realistically observe the details of changes of air flowing through the observation object, their high experimental costs, limited simulation range, and physical model accuracy requirements limit the popularity of this method. The CFD method is suitable for small-scale, high-resolution fluid simulations [27–29]. CFD is often used for industrial component design, building structure design, urban planning environment prediction, pollutant diffusion simulation, and the like. It has high reliability. However, due to the huge number of calculations involved, CFD is often used to simulate the wind environment of single, multibody, or small-scale building

groups. This method is not suitable for large-scale urban-level wind environment simulations.

The numerical simulation method uses GIS technology to analyze urban ventilation environments by calculating the surface roughness of the underlying surface [30–34]. Many studies have shown that this method can quickly and effectively analyze urban ventilation environments and is suitable for large-scale analysis of ventilation environments. Its implementation can be divided into two main approaches, one based on rules and the other based on a least-cost path analysis (hereafter, the LCP-based method) [35–37].

The rule-based method is based on the ventilation analysis results of small-scale building groups in wind tunnel experiments or CFD experiments. This method can obtain the relationship between urban morphological parameters (such as the frontal area index, or FAI) and ventilation conditions, establish a rule recognition model, and then use the model to analyze the ventilation environment of the entire city. The FAI is one of many surface roughness indicators. It represents the ratio of the projected area of the building on the normal plane of the wind direction to the projected area of the analysis region. The larger the value is, the greater the wind resistance is. Yuan [38] used the FAI to analyze the ventilation environment of Wuhan and obtained an intuitive result of potential air paths. The rule-based method is simple and easy to understand, which is conducive to implementation in planning, but under this method, it is particularly difficult to analyze the dynamic differences of urban ventilation environments under different background wind conditions.

Based on the roughness index, the LCP-based method uses a least-cost path analysis to obtain a more accurate ventilation corridor distribution. This method can dynamically analyze the ventilation corridors of the urban canopy following changes in wind direction. The LCP-based method assumes that the airflow always flows in the direction with the lowest wind resistance, and the path with the least accumulated wind resistance is the ventilation corridor [30]. Many constructive results have been obtained using the LCP-based method, confirming the credibility and correctness of this approach [30–32]. However, this method cannot effectively identify corridor width, and it is difficult to evaluate the ventilation conditions of places without least-cost paths (LCPs).

Based on the above analysis, a new ventilation corridor analysis method is urgently needed, which needs to meet the following requirements. First of all, this method should have a lower operating cost to implement the analysis of the urban ventilation environment in large areas. Secondly, this method should have the ability of ventilation environment analysis of dynamic wind direction. Then, the analysis results need to reflect the ventilation status of the whole study area, so as to analyze the impact of urban internal structure on ventilation environment. In this study, a ventilation environment analysis method based on the least cumulative ventilation cost (LCVC) is proposed. Taking Wuhan as a case study area, the feasibility and accuracy of the method are verified. The results show that the method can meet the above three requirements and can be used as a new tool for urban ventilation environment analysis.

2. Study Area

Wuhan is the capital city of Hubei Province with an area of 8589 km^2, located at 29°58′–31°22′ N and 113°41′–115°05′ E (Figure 1). Wuhan is located in the east of the Jianghan Plain and the middle reaches of the Yangtze River. The world's third-largest river, the Yangtze, and its largest tributary, the Han River, meet in the city, dividing Wuhan's central urban area into three parts. These are Hankou (including Jianghan District, Jiang'an District, and Qiaokou District), Wuchang (including Wuchang District, Qingshan District, and Hongshan District), and Hanyang. The rivers and lakes (such as the East Lake, Tangxun Lake, South Lake, and Sand Lake) are intricately woven into the fabric of the city. The water area occupies a quarter of the city's total area, providing the city with a lot of open spaces along the lakes and rivers.

Wuhan has a long history. In recent years, because it is a strategic development city in central China, the scale of its built-up areas has expanded rapidly. The mix of old and new urban areas has brought great difficulties to urban planning and environmental protection, however. Wuhan's UHI effect is gradually increasing, with the highest surface temperature (heat source center) reaching 58.7°C and the maximum surface temperature difference between cities and suburbs reaching 20°C. The problem of UHIs is an increasingly important issue that plagues urban development. Therefore, it is very important to research and solve the problems of urban ventilation in Wuhan.

3. Data

The fundamental geographic information database (including land use data, road network data, and 3D building data) and point of interest (POI) database were provided by the Wuhan Natural Resources and Planning Bureau (Table 1). The building coordinates, ground graphics, and building height information are contained in a 3D database that is used to calculate the ventilation resistance coefficient of buildings. Daily wind data for 2018 were provided by the China Meteorological Administration. Landsat 8 imagery for land surface temperature (LST) inversion was obtained from the United States Geological Survey (USGS).

4. Method

4.1. Methods for the Determination of Roughness Parameters. In air quality and meteorological models, surface roughness is used to express the drag effect of rough surfaces. Use of the morphometric method, which is based on surface roughness, for calculating wind profiles in urban boundary layers (UBLs), has been extensively studied [39, 40]. Using a current modeling method based on a 3D building database, Gal and Unger [41] studied the roughness (Z_0) of urban areas to analyze the urban wind environment. In order to make the assessment of urban air permeability more practical and to provide urban planners with computable

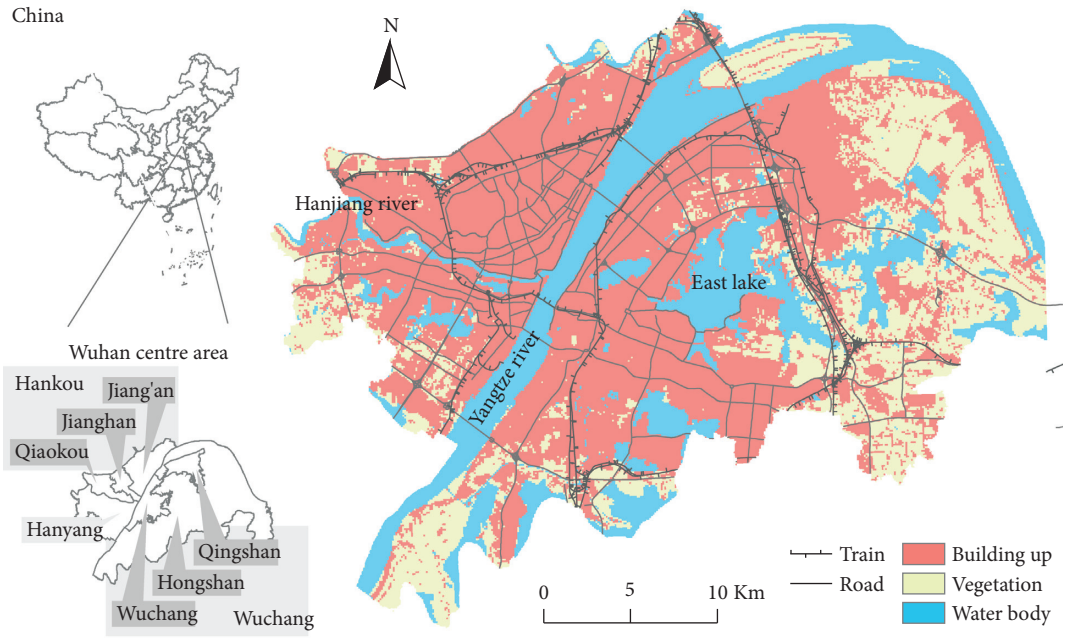

Figure 1: Map of the study area.

Table 1: The data sources.

Data	Type	Sources
Fundamental geographic information database	Vector	Wuhan Natural Resources and Planning Bureau
Daily wind data	Table	China Meteorological Administration
Landsat 8	Image	USGS
POI	Vector	Wuhan Natural Resources and Planning Bureau

geometric parameters of the city, many indices have been developed to assess urban permeability, such as the frontal area index λ_f and the site coverage ratio λ_p [30, 38, 42]. In this study, the frontal area index λ_f was selected as the roughness measurement index.

4.1.1. Calculation of the Frontal Area Index. Windward building walls obstruct airflow. The frontal area index is a measurement of the building frontal area facing into the wind. The frontal area index was first approximated by the product of the average height, width, and density of the buildings [39]:

$$\lambda_f = \overline{L_y H} \rho_d, \quad (1)$$

where $\overline{L_y}$ is the average width of the buildings perpendicular to the wind direction, $\overline{H}$ is the average height of buildings, and ρ_d is the density of buildings per unit area.

Burian [40] calculated the frontal area index in any wind direction directly using ArcView Avenus script and an improved formula:

$$\lambda_{f(\theta)} = \frac{A_{proj}}{A_T}, \quad (2)$$

where $\lambda_{f(\theta)}$ represents the frontal area index of buildings facing into the wind θ, A_{proj} represents the total projected area of buildings on a plane perpendicular to the wind direction, and A_T represents the plan area.

There is some ambiguity about the minimum distance between two adjacent buildings that divides them into two separate buildings. The problem is that as the two buildings get closer, the upwind building may begin to obscure the facade of the leeward building. Analyzing the exposed front area (shown in Figure 2) may be more important than analyzing the total front area [40]. Wong [30] eliminated the area blocked by buildings upwind of the blocked area of the leeward buildings by setting incremental projection lines (with an interval of 5 meters). In this study, a program was developed that was based on the ArcGIS 10.2 in the NET 4.0 environment. The projected areas of the buildings were directly integrated through a graphic method to calculate the frontal area index. The average frontal area index λ_f is obtained by weighting $\lambda_{f(\theta)}$ with annual frequency P_θ of wind direction θ. n is the collection of wind direction. In this paper, there are 16 wind directions, so $n = 16$. The equation is as follows:

$$\lambda_f = \sum_{\theta=1}^{n} \lambda_{f(\theta)} \cdot P_\theta. \quad (3)$$

4.1.2. Resolution. Recent studies have mainly used two aggregation methods. One is to aggregate buildings based on building blocks, which treats buildings as a unit. The other is to use a regular grid to process the building data, which is

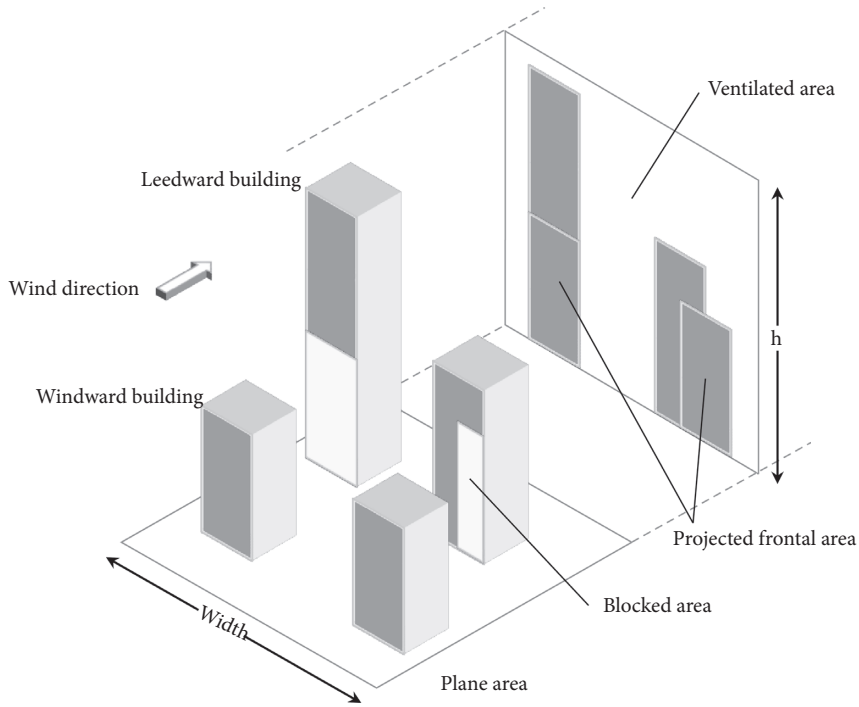

Figure 2: Diagram of the frontal area index.

often used for spatial data analysis. Open space is a key factor in assessing urban ventilation, but it cannot be expressed well using the building block aggregate method. Therefore, in this study, a regular grid was selected to divide the urban space [31].

Due to the scale effect, analyzing the same data at different scales will lead to different results. The selection of the grid scale should consider the correlation between the calculated value of the frontal area index and the actual ventilation capacity of the study area, as well as the ability of the frontal area index to express the details of ventilation [42]. Hsieh [31] conducted an urban ventilation study in Tainan using 100 m grids. The Hong Kong Planning Department found 100 m grids to be compatible with various variables for the thermal environment in urban climate research [30]. The correlation between the frontal area index and UHI intensity was analyzed using a grid scale from 400 m to 40 m in Hong Kong, and it was found that the two showed the highest correlation on the 100 m grid scale [30, 43]. A 100 m grid has been used to study the ventilation environment of Wuhan central urban area [38], which has the same research area as this study. In light of these research results, a 100 m regular grid was used to divide the research area in this study.

4.1.3. Zero Displacement Height. The morphometric method based on surface roughness for calculating wind profiles in UBLs has been studied extensively. Current morphology models, such as those of MacDonald [44] and Bottema [45], assume that wake interference between surface obstacles is negligible and that the average wind speed approaching each obstacle is logarithmic. Given these assumptions, these models are only valid when the frontal area index λ_f is less than 0.3–0.5. In other words, as the roughness increases, the average wind profile approaching each building becomes nonlogarithmic because the interference between buildings promotes air turbulence near the ground. This is why it is necessary to introduce zero displacement height (Z_d) into the logarithmic velocity profile.

MacDonald [44] proposed that the frontal area index above the displacement height (λ_f^*) can estimate Z_0 better than λ_f and proposed that the average wind speed below the displacement height be assumed to be zero. Ng [42]suggested that wind speed below Z_d might depend on building geometries such as λ_f' (frontal area density below Z_d) and used 15 m as the value of Z_d. Wong [30] further simplified the frontal area index under the displacement height. Z_d was set as 20 m indirectly by setting the lowest level interval of λ_f as (0, 0.2) within 100 m grids. The 3D building data used in this study do not include information on overpasses, large traffic billboards, and large green vegetation, and these are important details for calculating λ_f'. Therefore, this study extends Wang's method to set different Z_d values for different land types (Z_d^b = 10 m for built-up areas and Z_d^w = 1 m for water bodies).

4.2. LCVC Analysis. The LCP-based method has been considered feasible for identifying urban ventilation corridors. The LCP-based method assumes that the air always flows in the direction of least resistance, thus determining the path from the starting point to the end point on the ventilation resistance grid [30, 46]. In the LCP-based method, the Z_d value is defined as the resistance value. The higher the Z_d value is, the higher the resistance value is. In

addition, n starting points and m ending points are determined in order to represent the air inlets and air outlets, respectively. The LCP-based method is then used to generate $n * m$ LCPs between the start and end points. Finally, the LCP frequency of each grid is calculated. The higher the frequency is, the better the ventilation conditions are, and vice versa. This method can effectively identify the main ventilation corridors, but the disadvantages are also obvious, namely, the lack of estimation of corridor width and the inestimability of the grids with zero LPC frequency.

This study proposes a new approach, namely, the LCVC. For any ventilation resistance surface, let s be the air inlet, d be the air outlet, and m be a point on an LCP between s and d. Then, the LCVC from s to d through m can be written as the following formula:

$$C_{s\longrightarrow d|m} = C_{s\longrightarrow m} + C_{m\longrightarrow d}. \quad (4)$$

According to the calculation formula of $\lambda_{f(\theta)}$, the calculated values are equal when the difference of θ is π:

$$\lambda_{f(\theta)} = \lambda_{f(\pi-\theta)}. \quad (5)$$

Therefore, the values of LCVC from m to d and from d to m are equal, which can be expressed by the following formula:

$$C_{m\longrightarrow d} = C_{d\longrightarrow m}. \quad (6)$$

Combining equation (4) and equation (6) gives

$$C_{s\longrightarrow d|m} = C_{s\longrightarrow m} + C_{d\longrightarrow m}. \quad (7)$$

The smaller the value of $C_{s\longrightarrow d|m}$ is, the lower the cost of airflow passing through the m point is, and the better the ventilation condition is. Using equation (7), the cumulative ventilation cost values at any point to the air outlet and air inlet can easily be calculated, and the LCVC at that point can be obtained by superposition of the two. The average ventilation cost can be obtained by weighting the LCVC values with wind direction frequencies.

4.3. Ventilation Potential and Urban Functional Units. Different types of urban functional units are usually accompanied by different building structures and building heights. For example, residential areas are usually accompanied by middle- or high-rise buildings, and public areas are usually accompanied by low- or middle-level buildings. It is predicted that different urban functional units can be characterized by λ_f and ventilation cost. In this study, the urban functional unit information was obtained from the urban POI database.

4.4. Validation of Ventilation Cost. The LST is considered to be related to the urban ventilation environment [33]. In Qiao's research, LST was used to verify the results of the corridor analysis. This study uses LST inversed from Landsat 8 data to verify the results. Retrieve processing includes three main steps: from digital numbers to spectral radiation, from spectral radiation to sensor brightness temperature, and from sensor brightness temperature to LST. In this study, the retrieve processing was implemented by using the Landsat 8 Surface Temperature Inversion System (V2.0) developed by Ren Huazhong from the Institute of Remote Sensing and GIS, Peking University.

5. Results

5.1. Spatial Distribution of the Wind Resistance Coefficient. There are 101,328 buildings in the study area (Figure 3 and Table 2). The building height range is between 0 m and 204 m, with 57,720 buildings less than 10 m, accounting for 48.91% of the total building area. As the height increases, the number and area of the buildings gradually decrease. Buildings with a height between 10 m and 24 m account for 33.38% of the total number of buildings and 38.46% of the total building area. There are 9,663 buildings with a height between 24 m and 100 m, accounting for 12.48% of the total building area. There are 120 buildings higher than 100 m, accounting for only 0.12% of the total number of buildings.

The wind resistance coefficient obtained according to the method described in Section 4 is shown in Figure 4. The spatial distribution of the wind resistance coefficient is positively related to building height. The average wind resistance coefficient of all grids is 0.153. The number of grids containing high-rise buildings (height greater than 24 m) accounts for 30.26%, and the average wind resistance coefficient is 0.299. Qiaokou, Jianghan, Jiang'an, and Wuchang are the old urban areas of Wuhan. The average wind resistance coefficient of these districts is 0.177, and 0.298 for the grid containing high-rise buildings. Qingshan is an important heavy industry base. There are many single-story factories and middle-rise residential buildings in this area, so its average wind resistance coefficient is only 0.113. Hanyang and Hongshan are development zones, with an average wind resistance coefficient of 0.138.

In order to determine the wind resistance formed by different urban functional units and to prepare for the ventilation cost analysis, the resistance coefficients of 12 types of urban functional elements were calculated, as shown in Table 3. The urban functional units were obtained from the Wuhan POI database, which contains 155,421 POI points. The ventilation resistance coefficient of outdoor open spaces (parks, green spaces, and squares) was 0.111, which is significantly lower than that of other urban functional units. Next came public management and social organization units, with an average ventilation resistance coefficient of 0.199. Public services and companies had the highest ventilation resistance coefficients, with 0.251 and 0.243, respectively. These two types of units are usually accompanied by a strong financial correlation, which results in a higher spatial distribution consistency.

5.2. Statistics on Wind Direction and Frequency. When analyzing the urban ventilation conditions, the results for each standard wind direction need to be linearly weighted according to the actual wind direction frequency. The wind direction and frequency were thus plotted on a radar chart according to the daily meteorological statistics of Wuhan in

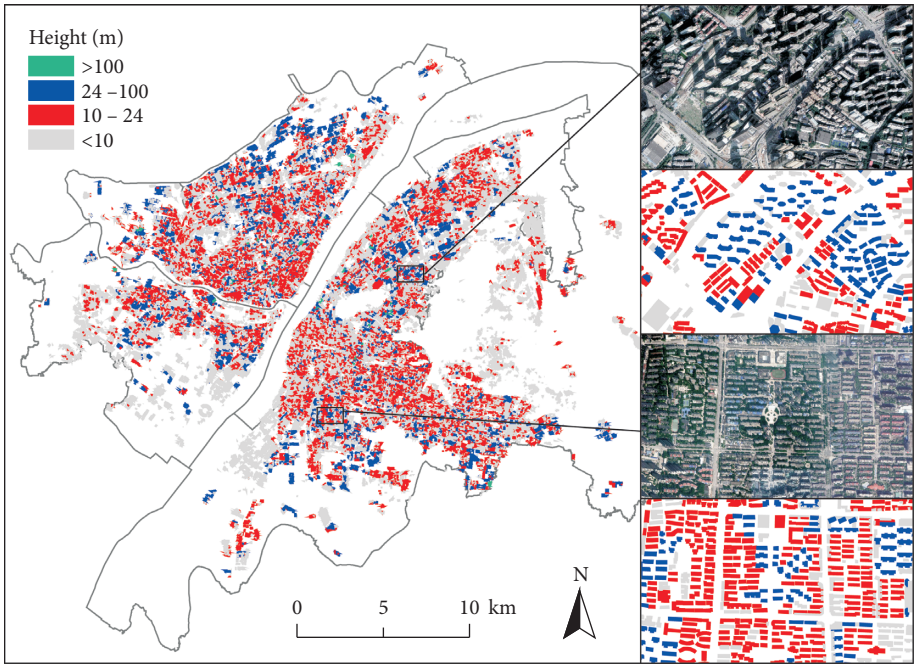

Figure 3: 3D spatial distribution of buildings.

Table 2: Height of buildings in the study area.

Height (m)	Number	Percentage of all buildings (%)	Building area (km^2)	Percentage of total building area (%)
$H \leq 10$	57720	56.96	32.14	48.91
$10 < H \leq 24$	33825	33.38	25.28	38.46
$24 < H \leq 100$	9663	9.54	8.20	12.48
$100 < H$	120	0.12	0.10	0.15

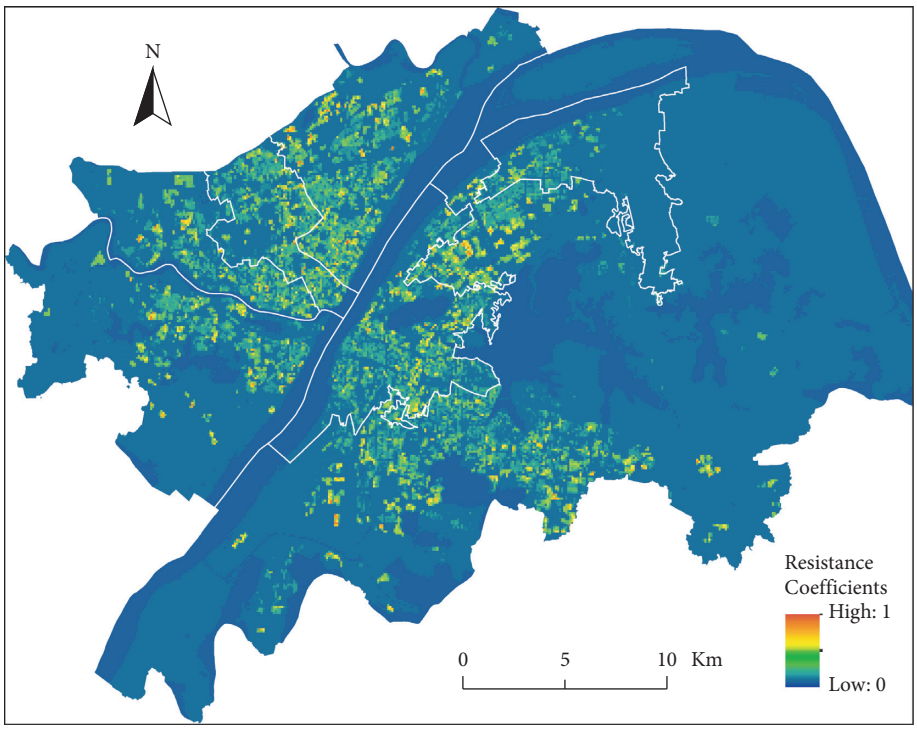

Figure 4: Resistance coefficients map.

Table 3: Classification of urban functional elements and average resistance coefficients in Wuhan.

Reclassification	Description	Resistance
Public management and social organizations	Government, welfare agency, revenue, financial bureau, jurisdiction bureau, administration for industry and village, fire control, police station, court, etc.	0.199
Residential districts	Residential district, villa, dormitory, etc.	0.215
Commerce	Commercial building, supermarket, shopping center, market, small store, grocery, etc.	0.214
Factories	Various types of manufacturing factory and technology enterprise	0.184
Companies	Company, law office, accountant office, audit office, tourist agency, insurance company, consulting corporation, etc.	0.243
Public services	Bank, post office, telecom bureau, postal bank, etc.	0.251
Everyday services	Hairdressing, public bathroom, laundry, tailor, car repair or wash shop, etc.	0.224
Hotels	Hotel, restaurant, snack, cafe, teahouse, etc.	0.212
Educational institutions	University, college, middle school, primary school, kindergarten, training center, private school, etc.	0.216
Medical institutions	Hospital, children's hospital, clinic, emergency center, psychiatric hospital, eye hospital, bone hospital, dental clinic, pharmacy, etc.	0.217
Outdoor open areas	Park, square, botanic garden, amusement park, resort, agricultural center, etc.	0.111
Transportation facilities	Railway station, bus station, coach station, parking lot, etc.	0.209

2018 (Figure 5). The main wind direction is northerly (including N, NE, NW, NNW, and WNW), followed by southeasterly (including E, SE, SSE, and ESE). Affected by the monsoon climate, the dominant wind direction varies from season to season. The prevailing winds affected by the northern cold in the autumn and winter are mainly north winds (including N, NE, NW, and NNE), followed by a few east winds (including E, NE, ENE, and SE). The meteorological changes in spring are complicated, and the prevailing winds are still mainly northerly, followed by southeasterly (including ESE and SSE). In summer, the northerly and southwesterly winds (SW, WSW, and SSW) are similar in frequency and accompanied by a few southeasterly winds.

5.3. Results of LCVC Analysis. The difference in wind direction frequency indicates the variation in the influence of the LCVC in each wind direction. Given a time interval, the average LCVC is obtained by weighting the LCVC of each wind direction with the corresponding frequency.

Figure 6 shows the results for the LCVC analysis of 16 wind directions in the urban center of Wuhan. In order to maintain comparability, the calculation results of different wind directions use the same classifications and map colors. Red indicates high ventilation costs and blue indicates low ventilation costs. The coherent narrow passages formed by the low-cost areas are the ventilation corridors. Generally speaking, the ventilation costs around the city and in open areas are less than those in densely populated areas. Affected by different wind directions, the spatial distribution of ventilation corridors in the city takes on different shapes, and the directionality of the corridors is consistent with the wind direction. For the wind directions of NNE, NE, SSE, and SW, the Yangtze River is the most important urban ventilation corridor. For the wind directions of E, ESE, W, and WNW, the interconnected open space formed by the Han River and the East Lake forms the main ventilation corridor.

The spatial distribution of the LCVC in the different seasons in Wuhan is shown in Figure 7. Seasonal LCVCs are normalized and divided into 10 levels. Colors from blue to red indicate higher ventilation costs. Overall, the distribution patterns of the LCVCs are very similar in the four seasons. The dominant wind direction of Wuhan throughout the year is NNE (N, NNE, and NE). The Yangtze River runs through the city and forms the main NE-SW ventilation corridor, with its open waters and north-south connectivity. Two islands with high ventilation costs, centered on Hankou and Wuchang, are formed along the east and west sides of the Yangtze River. The areas of the two are equivalent, but the Hankou side presents a single-core model and the area of high-value areas is large. By contrast, the Wuchang side presents a multicore model, and the area of high-value areas is small and scattered. The East Lake has become another important urban ventilation corridor due to its large water area and its distribution deep into the city's hinterland. There are also some differences in the distributions of LCVCs in different seasons. In summer, due to the high wind frequency in an N-S direction, the ventilation corridor formed by the Yangtze River is more obvious than in other seasons. In winter, the width of the ventilation corridor in the north of the East Lake is slightly narrower than in other seasons. At the same time, the width of the ventilation corridors formed by the middle-level LCVC area (from 5 to 7) was also narrower than in other seasons or even disappeared. In the spring and autumn, when the frequency of the south wind is slightly higher than in winter and summer, the ventilation corridors running in an S-N is more obvious.

Summarized below are the details of the spatial distribution pattern of ventilation costs and the three levels of ventilation corridors identified, namely, the main, secondary, and capillary levels.

The main ventilation corridors lay the foundation for urban ventilation. The distribution of the main ventilation corridors has a high spatial correlation with natural geographical features (such as rivers and lakes). The results show that there are two main ventilation corridors in central Wuhan. One is the NE-SW corridor formed by the Yangtze River, and the other is the S-N and NW-SE corridor formed by the East Lake. The secondary ventilation corridors are mostly connected to the main ventilation corridors, and

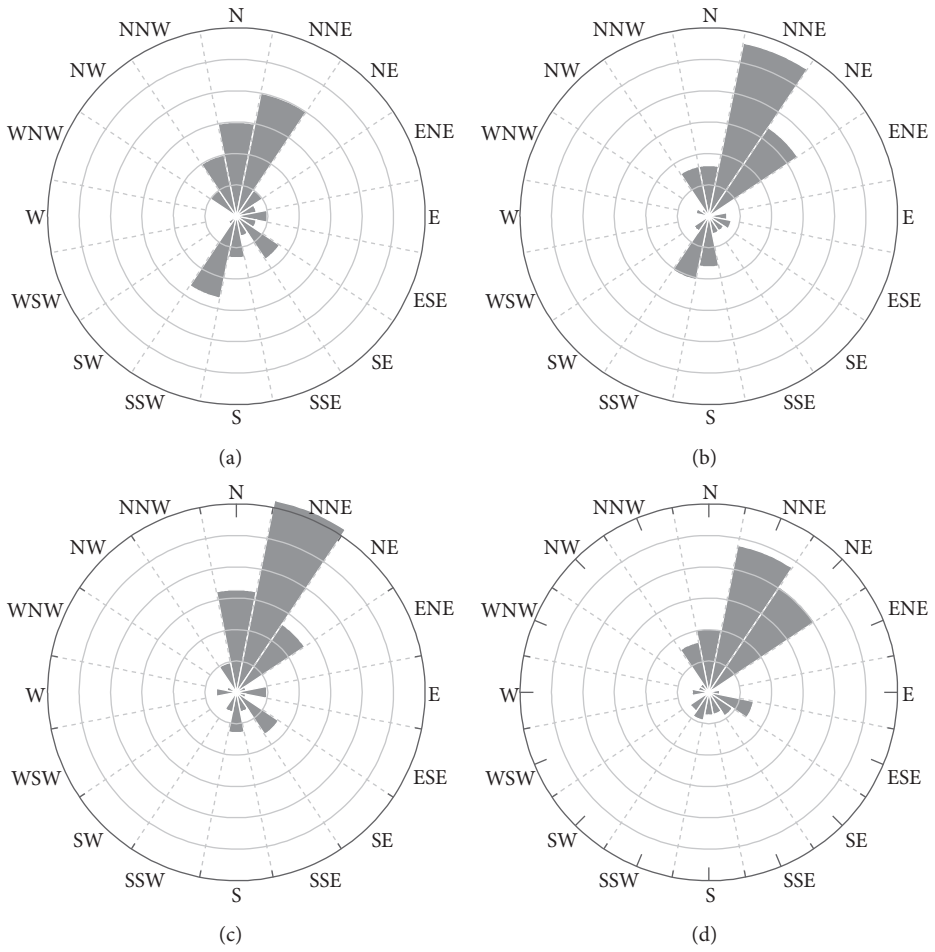

Figure 5: A wind-rose diagram for each season in Wuhan. (a) Spring. (b) Summer. (c) Autumn. (d) Winter.

their distribution is affected by the main ventilation corridors. The secondary ventilation corridors spatially divide the high ventilation cost area into several subareas, which play an important part in promoting urban ventilation. Depending on the main ventilation corridors of the East Lake, many N-S or SE-NW secondary ventilation corridors are formed in Wuchang District, Qingshan District, and Hongshan District. These ventilation corridors promote ventilation in these three areas. The secondary ventilation corridor formed by the Han River connects to the main ventilation corridor formed by the Yangtze River, which promotes the ventilation conditions in Hanyang.

Capillary ventilation corridors are distributed in areas with high ventilation costs, and the areas with maximum ventilation costs are divided into several subregions. Capillary ventilation corridors cannot determine the overall conditions of regional ventilation but can effectively reduce the distribution of the maximum value of ventilation costs and can be used as a supplementary means for secondary ventilation corridors. Due to the large amount of capillary ventilation corridors, their locations are not marked on the map. It is easy to determine that the number of capillary ventilation corridors in Hankou (Wuchang District, Qingshan District, and Hongshan District) is significantly less than in Wuchang (Qiaokou District, Jianghan District, and Jiang'an District).

The ventilation cost distribution map enables the visualization of urban ventilation conditions. For example, blue indicates a low ventilation cost area, and red indicates a high ventilation cost area. Relatively low-cost areas between high costs are potential ventilation corridors. This facilitates a better understanding of urban ventilation conditions on both local and global scales. The frontal area index λ_f was performed on a local scale. When considering the entire urban area, due to the complexity of the buildings and the road network, it will be difficult to achieve the identification of ventilation corridors by visual inspection of the buildings and the windward index map [30]. The results of the LCVC method cover the entire research area, thus solving the problem of no-path passages in some areas in the traditional LCP method.

5.4. Validation of the LCVC Method. LST is related to ventilation conditions. When the ventilation conditions are good, the average surface is usually lower. The areas with poor ventilation conditions have a higher average surface temperature and less heterogeneity than other areas do. To verify the accuracy of the urban ventilation analysis, LST

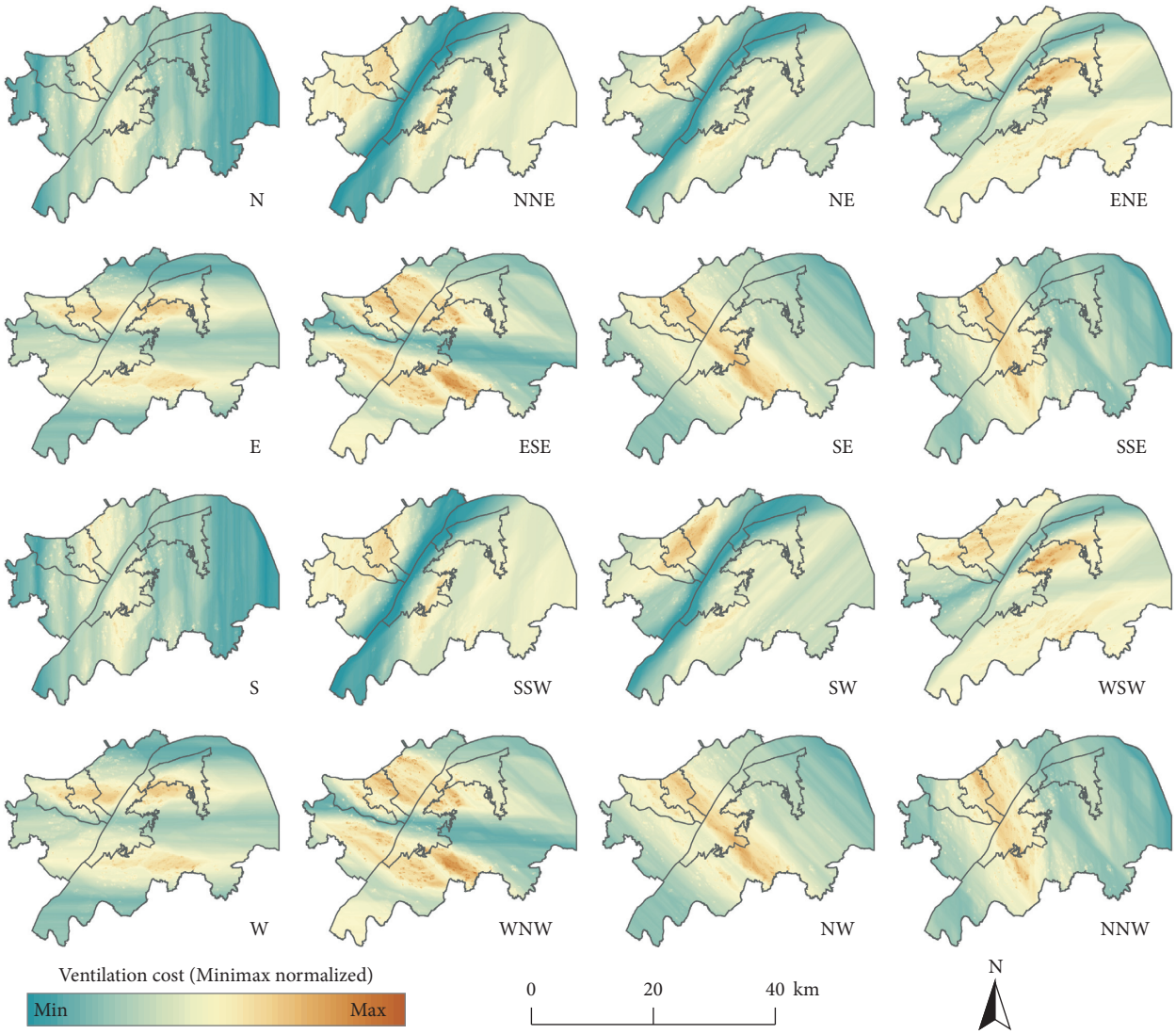

Figure 6: Spatial distribution of LCVC in different wind directions.

inversion was performed on the Landsat 8 data (Figure 8). By combining the LST map with the summer urban ventilation analysis results (Figure 7(b)), the LST values for different levels of ventilation costs were calculated (Table 4).

The results show that the average LST of the area with the best ventilation conditions is 34.19°C, significantly lower than that of other areas. The average LST in the area with the worst ventilation conditions is 40.53°C. In addition, the area with the worst ventilation conditions has less heterogeneity than other areas do, and the LST standard deviation is 1.71. As ventilation conditions improve, the LST standard deviation continues to increase.

5.5. Urban Ventilation Conditions and POIs. Table 5 shows the average ventilation costs for functional urban units. The average ventilation costs of outdoor open areas are obviously lower than the others, at only 0.469. The ventilation costs are highest for public service units, with a value of 0.568. This is mainly because these units are distributed in the main core areas of the city. The ventilation costs for the residential units are 0.559 in the second order, which is different from the ventilation resistance coefficient ranking. Residential units are usually larger and have a higher building density, resulting in higher ventilation costs. The ventilation costs of educational institutions are 0.554, similar to those for residential units. The majority of educational institutions are primary, secondary, high school, and training institutions. Most of these institutions are spatially associated with densely populated areas and therefore have similar ventilation costs to residential areas. Residential units are the main places where people live and usually have a high population density. Higher ventilation costs easily form heat islands and are not conducive to the spread of pollution, which affects people's health and quality of life. Therefore, in urban planning, the construction of outdoor open spaces in

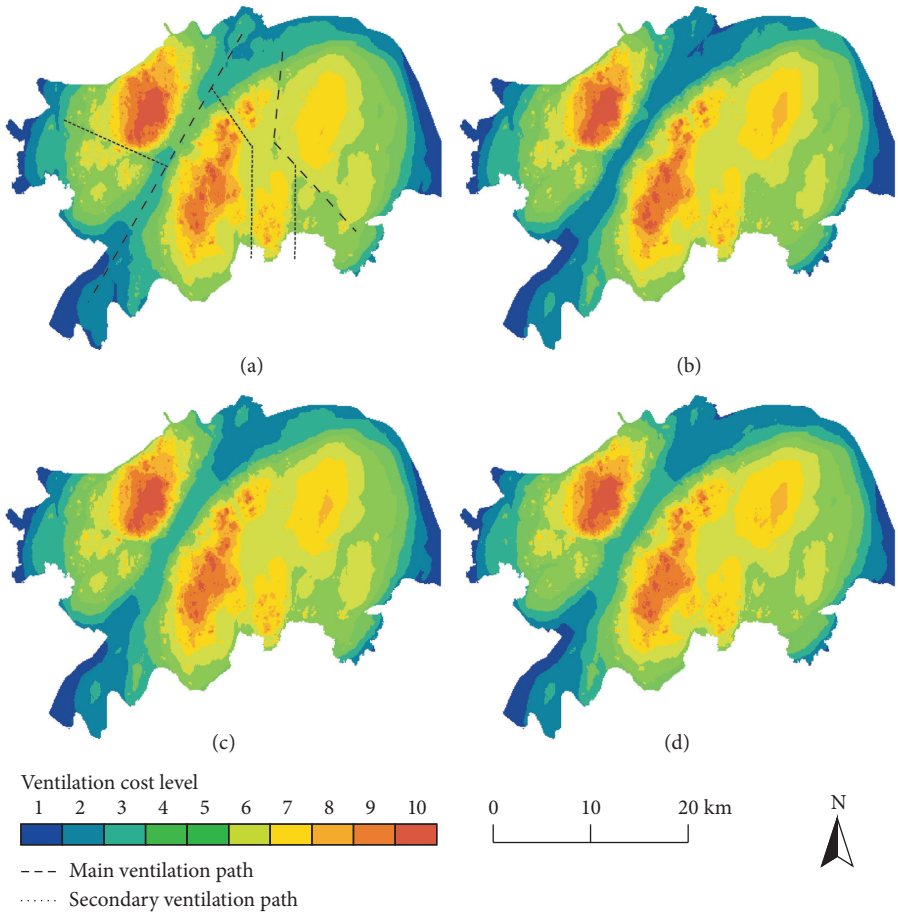

Figure 7: Spatial distribution of ventilation during different seasons. (a) Spring. (b) Summer. (c) Autumn. (d) Winter.

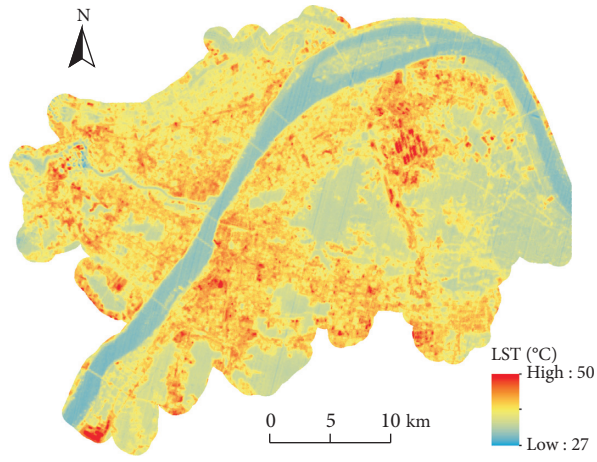

Figure 8: Spatial distribution of LST in summer.

Table 4: Statistical characteristics of LST at different levels of ventilation cost.

Ventilation levels	Temperature (°C)				
	Lowest	Highest	Range	Average	Standard deviation
2	29.28	50.46	21.18	34.19	3.64
3	28.17	52.59	24.42	34.96	3.74
4	29.67	55.99	26.32	37.69	4.05
5	29.16	49.47	20.31	38.82	3.24
6	31.89	56.17	24.28	38.07	3.24
7	32.10	50.24	18.14	37.95	3.35
8	32.85	55.55	22.70	40.08	3.02
9	32.50	54.70	22.20	40.12	2.60
10	34.34	50.73	16.39	40.42	2.05
11	34.66	46.83	12.17	40.53	1.71

Table 5: Urban functional units and average ventilation costs.

Reclassification	Ventilation cost
Public management and social organizations	0.535
Residential districts	0.559
Commerce	0.519
Factories	0.483
Companies	0.545
Public services	0.568
Everyday services	0.545
Hotels	0.538
Educational institutions	0.554
Medical institutions	0.544
Outdoor open areas	0.469
Transportation facilities	0.541

residential areas should be strengthened to improve the ventilation environment.

6. Discussion and Conclusion

Using the urban morphological characteristics identified by GIS technology, this study established an LCVC method to describe quantitatively the urban ventilation environment at the city scale. First, the frontal area index of three-dimensional urban buildings representing the ventilation resistance coefficient was calculated using a morphological method. Second, the minimum cumulative ventilation cost algorithm was applied to draw the urban ventilation cost maps under different wind directions. Then, the wind frequency weighting was used to explore the urban ventilation environment in different seasons, and the urban ventilation corridors of different levels were analyzed. Finally, the results of the summer ventilation analysis were verified using the LST retrieved from Landsat 8 data.

The analysis of the urban ventilation environment based on the morphology and GIS technology has the advantage of high calculation efficiency. In addition, the results of the analysis are highly compatible with other spatial analysis and mapping technologies. This study proposes that the cumulative costs of ventilation can better reflect the differences in urban ventilation conditions than the ventilation resistance coefficient can. In contrast to the corridor extraction method based on empirical rules, the proposed method can directly observe the dynamic characteristics of urban ventilation under different wind directions and frequencies. In contrast to the least-cost path analysis method, the results of the LCVC method cover the whole study area, and the corridor width and area can also be measured. However, several issues require further study. The urban wind environment is affected not only by ground roughness but also by atmospheric environment and local temperature factors. Therefore, it is difficult to achieve an accurate analysis of local wind speeds and directions from an analysis of building form alone. In addition, it is difficult to obtain internal high-density real-time wind speed data, especially wind speed measurements in a vertical direction. This makes it difficult to improve the model parameters. These issues will be further studied.

Data Availability

The data used to support the findings of the study are available from the corresponding author upon request.

Conflicts of Interest

The authors declare that they have no conflicts of interest.

Acknowledgments

This study was supported by the National Key Research and Development Program of China (Grant no. 2017YFB0503601) and China Postdoctoral Science Foundation (Grant no. 2019M662726).

References

[1] H. Wang, G. Wang, J. Qi et al., "Scarcity-weighted fossil fuel footprint of China at the provincial level," *Applied Energy*, vol. 258, 2020.

[2] L. Jiang, B. Xue, Z. Ma, L. Yu, B. Huang, and X. Chen, "A life-cycle based co-benefits analysis of biomass pellet production in China," *Renewable Energy*, vol. 154, pp. 445–452, 2020.

[3] H. Wang, H. Schandl, G. Wang, and L. Ma, "Regional material flow accounts for China: examining China's natural resource use at the provincial and national level," *Research and Analysis*, vol. 6, 2019.

[4] B.-J. He, Z.-Q. Zhao, L.-D. Shen, H.-B. Wang, and L.-G. Li, "An approach to examining performances of cool/hot sources in mitigating/enhancing land surface temperature under different temperature backgrounds based on landsat 8 image," *Sustainable Cities and Society*, vol. 44, pp. 416–427, 2019.

[5] B.-J. He, L. Yang, and M. Ye, "Strategies for creating good wind environment around Chinese residences," *Sustainable Cities and Society*, vol. 10, pp. 174–183, 2014.

[6] H. Akbari, C. Cartalis, D. Kolokotsa et al., "Local climate change and urban heat island mitigation techniques–the state of the art," *Journal of Civil Engineering and Management*, vol. 22, no. 1, pp. 1–16, 2016.

[7] D. Zhou, L. Zhang, L. Hao, G. Sun, Y. Liu, and C. Zhu, "Spatiotemporal trends of urban heat island effect along the

urban development intensity gradient in China," *Science of The Total Environment*, vol. 544, pp. 617–626, 2016.

[8] D. Zhou, S. Zhao, L. Zhang, G. Sun, and Y. Liu, "The footprint of urban heat island effect in China," *Scientific Reports*, vol. 5, p. 11160, 2015.

[9] K. Zhang, Y. Chen, and L. Wu, "Grey spectrum analysis of air quality index and housing price in Handan," *Complexity*, vol. 2019, 2019.

[10] Y. Zhao, Y. Li, and Q. Chen, "Analysis of a stochastic susceptible-infective epidemic model in a polluted atmospheric environment," *Complexity*, vol. 2019, 2019.

[11] W. Zhang, C. M. Mak, Z. T. Ai, and W. M. Siu, "A study of the ventilation and thermal comfort of the environment surrounding a new university building under construction," *Indoor and Built Environment*, vol. 21, no. 4, pp. 568–582, 2011.

[12] R. A. W. Albers, P. R. Bosch, B. Blocken et al., "Overview of challenges and achievements in the climate adaptation of cities and in the Climate Proof Cities program," *Building and Environment*, vol. 83, pp. 1–10, 2015.

[13] L. W. A. van Hove, C. M. J. Jacobs, B. G. Heusinkveld, J. A. Elbers, B. L. van Driel, and A. A. M. Holtslag, "Temporal and spatial variability of urban heat island and thermal comfort within the Rotterdam agglomeration," *Building and Environment*, vol. 83, pp. 91–103, 2015.

[14] A. Guo, J. Yang, X. Xiao, J. Xia, C. Jin, and X. Li, "Influences of urban spatial form on urban heat island effects at the community level in China," *Sustainable Cities and Society*, vol. 53, 2020.

[15] Z.-Q. Zhao, B.-J. He, L.-G. Li, H.-B. Wang, and A. Darko, "Profile and concentric zonal analysis of relationships between land use/land cover and land surface temperature: case study of Shenyang, China," *Energy and Buildings*, vol. 155, pp. 282–295, 2017.

[16] E. Ng, "Policies and technical guidelines for urban planning of high-density cities—air ventilation assessment (AVA) of Hong Kong," *Building and Environment*, vol. 44, no. 7, pp. 1478–1488, 2009.

[17] B. Chun and J.-M. Guldmann, "Spatial statistical analysis and simulation of the urban heat island in high-density central cities," *Landscape and Urban Planning*, vol. 125, pp. 76–88, 2014.

[18] Y. He, A. Tablada, and N. H. Wong, "A parametric study of angular road patterns on pedestrian ventilation in high-density urban areas," *Building and Environment*, vol. 151, pp. 251–267, 2019.

[19] J. Yang, Y. Wang, X. Xiao, C. Jin, J. Xia, and X. Li, "Spatial differentiation of urban wind and thermal environment in different grid sizes," *Urban Climate*, vol. 28, 2019.

[20] J. Yang, S. Jin, X. Xiao et al., "Local climate zone ventilation and urban land surface temperatures: towards a performance-based and wind-sensitive planning proposal in megacities," *Sustainable Cities and Society*, vol. 47, 2019.

[21] Z. Qiao, L. Liu, Y. Qin et al., "The impact of urban renewal on land surface temperature changes: a case study in the main city of guangzhou, China," *Remote Sensing*, vol. 12, no. 5, ,.

[22] Z. Qiao, C. Wu, D. Zhao et al., "Determining the boundary and probability of surface urban heat island footprint based on a logistic model," *Remote Sensing*, vol. 11, no. 11, 2019.

[23] Z. Qiao, X. Xu, M. Zhao, F. Wang, and L. Liu, "The application of a binary division procedure to the classification of forest subcategories using MODIS time-series data during 2000-2010 in China," *International Journal of Remote Sensing*, vol. 37, no. 10, pp. 2433–2450, 2016.

[24] M. Bady, S. Kato, T. Takahashi, and H. Huang, "An experimental investigation of the wind environment and air quality within a densely populated urban street canyon," *Journal of Wind Engineering and Industrial Aerodynamics*, vol. 99, no. 8, pp. 857–867, 2011.

[25] M. Carpentieri, P. Salizzoni, A. Robins, and L. Soulhac, "Evaluation of a neighbourhood scale, street network dispersion model through comparison with wind tunnel data," *Environmental Modelling & Software*, vol. 37, pp. 110–124, 2012.

[26] K. T. Tse, A. U. Weerasuriya, X. Zhang, S. Li, and K. C. S. Kwok, "Pedestrian-level wind environment around isolated buildings under the influence of twisted wind flows," *Journal of Wind Engineering and Industrial Aerodynamics*, vol. 162, pp. 12–23, 2017.

[27] H. Montazeri, B. Blocken, and J. L. M. Hensen, "Evaporative cooling by water spray systems: CFD simulation, experimental validation and sensitivity analysis," *Building and Environment*, vol. 83, pp. 129–141, 2015.

[28] X. Wang and Y. Li, "Predicting urban heat island circulation using CFD," *Building and Environment*, vol. 99, pp. 82–97, 2016.

[29] K. R. Gautam, L. Rong, G. Zhang, and M. Abkar, "Comparison of analysis methods for wind-driven cross ventilation through large openings," *Building and Environment*, vol. 154, pp. 375–388, 2019.

[30] M. S. Wong, J. E. Nichol, P. H. To, and J. Wang, "A simple method for designation of urban ventilation corridors and its application to urban heat island analysis," *Building and Environment*, vol. 45, no. 8, pp. 1880–1889, 2010.

[31] C.-M. Hsieh and H.-C. Huang, "Mitigating urban heat islands: a method to identify potential wind corridor for cooling and ventilation," *Computers, Environment and Urban Systems*, vol. 57, pp. 130–143, 2016.

[32] S. Ling Chen, J. Lu, and W. W. Yu, "A quantitative method to detect the ventilation paths in a mountainous urban city for urban planning: a case study in Guizhou, China," *Indoor and Built Environment*, vol. 26, no. 3, pp. 422–437, 2017.

[33] Z. Qiao, X. Xu, F. Wu et al., "Urban ventilation network model: a case study of the core zone of capital function in Beijing metropolitan area," *Journal of Cleaner Production*, vol. 168, pp. 526–535, 2017.

[34] J. Yang, J. Sun, Q. Ge, and X. Li, "Assessing the impacts of urbanization-associated green space on urban land surface temperature: a case study of Dalian, China," *Urban Forestry & Urban Greening*, vol. 22, pp. 1–10, 2017.

[35] J. Srebric, M. Heidarinejad, and J. Liu, "Building neighborhood emerging properties and their impacts on multi-scale modeling of building energy and airflows," *Building and Environment*, vol. 91, pp. 246–262, 2015.

[36] X. Yang and Y. Li, "The impact of building density and building height heterogeneity on average urban albedo and street surface temperature," *Building and Environment*, vol. 90, pp. 146–156, 2015.

[37] F. Peng, M. S. Wong, Y. Wan, and J. E. Nichol, "Modeling of urban wind ventilation using high resolution airborne LiDAR data," *Computers, Environment and Urban Systems*, vol. 64, pp. 81–90, 2017.

[38] C. Yuan, C. Ren, and E. Ng, "GIS-based surface roughness evaluation in the urban planning system to improve the wind environment—a study in Wuhan, China," *Urban Climate*, vol. 10, pp. 585–593, 2014.

[39] C. S. B. Grimmond and T. R. Oke, "Aerodynamic properties of urban areas derived from analysis of surface form," *Journal of Applied Meteorology*, vol. 38, no. 9, pp. 1262–1292, 1999.

[40] S. J. Burian, M. J. Brown, and S. P. Linger, "Morphological analyses using 3D building databases: los Angeles, California," *Los Alamos National Laboratory*, vol. 74, 2002.

[41] T. Gál and J. Unger, "Detection of ventilation paths using high-resolution roughness parameter mapping in a large urban area," *Building and Environment*, vol. 44, no. 1, pp. 198–206, 2009.

[42] E. Ng, C. Yuan, L. Chen, C. Ren, and J. C. H. Fung, "Improving the wind environment in high-density cities by understanding urban morphology and surface roughness: a study in Hong Kong," *Landscape and Urban Planning*, vol. 101, no. 1, pp. 59–74, 2011.

[43] M. S. Wong and J. E. Nichol, "Spatial variability of frontal area index and its relationship with urban heat island intensity," *International Journal of Remote Sensing*, vol. 34, no. 3, pp. 885–896, 2013.

[44] R. W. Macdonald, R. F. Griffiths, and D. J. Hall, "An improved method for the estimation of surface roughness of obstacle arrays," *Atmospheric Environment*, vol. 32, no. 11, pp. 1857–1864, 1998.

[45] M. Bottema and P. G. Mestayer, "Urban roughness mapping—validation techniques and some first results," *Journal of Wind Engineering and Industrial Aerodynamics*, vol. 74–76, pp. 163–173, 1998.

[46] S. Ling Chen, J. Lu, and W. W. Yu, "A quantitative method to detect the ventilation paths in a mountainous urban city for urban planning: a case study in Guizhou, China," *Indoor Built Environment*, vol. 26, no. 3, pp. 422–437, 2017.